



## The major magnetic storm of March 13-14, 1989 and associated ionosphere effects

F. J. RICH AND W. F. DENIG

U.S. Air Force Phillips Laboratory, Geophysics Directorate, Space Physics Division, Hanscom Air Force Base, Bedford, MA 01731-5000, U.S.A.

Received October 1, 1991

The geomagnetic storm of March 1989 was the largest geomagnetic storm of the decade and one of the largest of the century. We review many of the "high-latitude" ionospheric observations that were made during this storm. Most of the data presented here comes from the polar-orbiting satellites of the Defense Meteorological Satellite Program (DMSP) series. A review of the DMSP data shows that most of the high-latitude, top-side ionospheric disturbance occurred on March 13 and 14. The magnitudes of the particle energy flux ( $\text{ergs cm}^{-2}$ ) ( $1 \text{ erg} = 10^{-7} \text{ J}$ ) and Joule heating were not unusually large for a storm, but the area of the energy deposition, and thus the total energy deposition, was extremely large. At the peak of the storm (minimum in  $D_u$  (disturbance with storm time) and midnight boundary indices) the auroral particle precipitation extended down to magnetic latitudes of  $40.1^\circ$  or  $L = 1.71$  while the polar edge of the auroral zone expanded poleward only slightly. The storm was also a period of intense, hemispherically symmetric polar rain fluxes. The auroral electric field was clearly observed down to magnetic latitude of  $35^\circ$ . This is consistent with the auroral electrojet (AE) current density and the AE index having a saturation level beyond which the index will increase slowly or not at all as more energy is transferred from the solar wind to the magnetosphere, but the cross polar-cap potential during this storm shows no evidence of saturation. There are only two visible light images from DMSP available near the peak of the storm. These images and one UV image from the Dynamics Explorer (DE) satellite at approximately the same time show the distribution of the aurora just after the peak of the storm. Comparison of the DMSP particle data with the DE-1 UV image indicates that the bifurcation of the auroral luminosity in the UV image is probably an effect of the DE-1 UV instrument's sensitivity limits; the DMSP data show no evidence for bifurcation of the auroral zone.

L'orage géomagnétique de mars 1989 fut le plus violent de la décennie et l'un des plus violents du siècle. Nous présentons une rétrospective de plusieurs des observations ionosphériques en haute altitude faites lors de cet orage. La plupart des données présentées ici proviennent des satellites en orbite polaire de la série DMSP. Ces données démontrent que le gros des perturbations ionosphériques en haute altitude eut lieu les 13 et 14 mars. Le flux d'énergie des particules (en  $\text{erg cm}^{-2}$  ( $1 \text{ erg} = 10^{-7} \text{ J}$ )) et le transfert de chaleur n'avaient pas une magnitude inhabituelle, mais la superficie affectée par le dépôt d'énergie, et par conséquent le dépôt d'énergie lui-même, furent immenses. Au plus fort de l'orage (minimum du  $D_u$  et des indices de frontière de minuit) la précipitation des particules aurorales s'étendait jusqu'aux latitudes magnétiques de  $40,1^\circ$  ou  $L = 1,71$ , tandis que du côté polaire l'aurore ne s'étendait que légèrement vers les pôles. L'orage fut aussi une période d'intense flux de pluie polaire à symétrie hémisphérique. On observa clairement le champ électrique auroral jusqu'à une latitude magnétique de  $35^\circ$ . Cela concorde avec une densité de courant d'électrojet auroral et un indice AE ayant un niveau de saturation, au-delà duquel l'indice croît lentement (ou pas du tout) lorsqu'augmente le transfert d'énergie du vent solaire à la magnétosphère, alors qu'il n'y a pas apparence d'une telle saturation dans le potentiel entourant le pôle. De l'orage à son plus fort, seulement deux images en lumière visible provenant du DMSP sont disponibles. Celles-ci et une image UV provenant du satellite DE au même moment montrent la distribution de l'aurore tout juste après le maximum de l'orage. Une comparaison des données en particules du DMSP avec l'image UV de DE-1 indique que la bifurcation de la luminosité aurorale dans l'image UV provient probablement de limites de sensibilité des appareils UV de DE-1. Les données du DMSP n'indiquent aucune bifurcation de la zone aurorale.

[Traduit par la rédaction]

Can. J. Phys. 70, 510 (1992)

93 7 22 041

### Introduction

The "great" geomagnetic storm of March 1989 produced some of the largest observed magnetic deflections of any storm in the past century (1). This storm produced significant disruptions in daily life and commerce in some parts of the world. Probably the most dramatic effect was the shut-down of the electric utility grid for the entire province of Quebec, Canada at 0742 UT on 13 March 1989 (2). Other effects, which are usually associated with large storms, were observed: the Global Positioning System (GPS) was disrupted (3), high-frequency (HF) radio communications were disrupted, low-altitude satellites dropped in altitude owing to increased drag and geosynchronous satellites experienced electronic upsets due to increased energetic particle fluxes (1).

Geomagnetic storms produce effects in the upper atmosphere, ionosphere, magnetosphere, and at all latitudes and all local times. The observed effects near the Earth's surface at low latitudes, mid-latitudes, and high latitudes are different, and are often studied as different phenomena, but they are all related. The degree and nature of the various storm-induced

effects are governed by several factors, including the maximum magnetic deflections (which is a measure of the ring current strength), the minimum latitude of the auroral zones (which is a measure of the strength of the process that injects plasma into the inner magnetosphere), the minimum radial distance of the magnetopause (which is a measure of the solar-wind dynamic pressure), and the rapidness with which the storm begins (which is influenced by the jump conditions at the shock front traveling in the solar wind and by the orientation of the interplanetary magnetic field (IMF)). These effects are all related, but the relationships are complex.

In this paper we describe some of the available ionospheric data over the high-latitude regions during the March 1989 storm, and compare these data with observations made during an "ordinary" storm. The majority of data for this report come from the Defense Meteorological Satellite Program (DMSP) Flight 8 (F8) and Flight 9 (F9) satellites partly because we maintain an archive of DMSP data and partly because data from other sources were either not available (e.g., the Millstone Hill incoherent radar was down for repairs during the storm) or were

93-16607  
1691

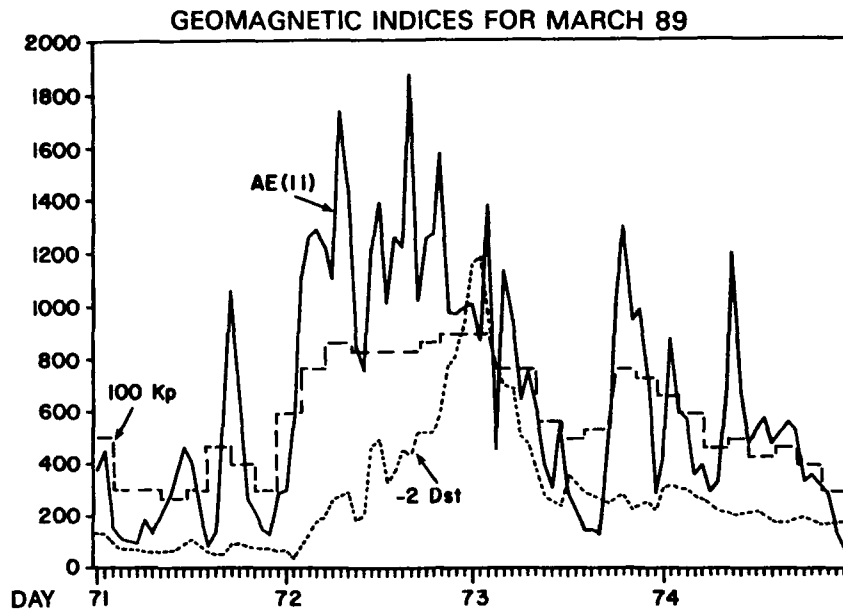


FIG. 1. The standard indices of geomagnetic activity before and during the great storm of March 1989. The high-latitude magnetic index AE, which indicates the strength and duration of substorm activity was derived from only 11 stations and will be revised when more complete data are available. The mid- to high-latitude magnetic index  $K_p$  indicates the general level of activity, but it saturates at a level of  $9^\circ$ . The  $K_p$  values plotted are multiplied by 100 to match the scale of the AE index. The low-latitude magnetic index  $D_{st}$  indicates the strength of the ring current in the inner magnetosphere. The  $D_{st}$  has been multiplied by  $-2$  to match the scale of the AE index.

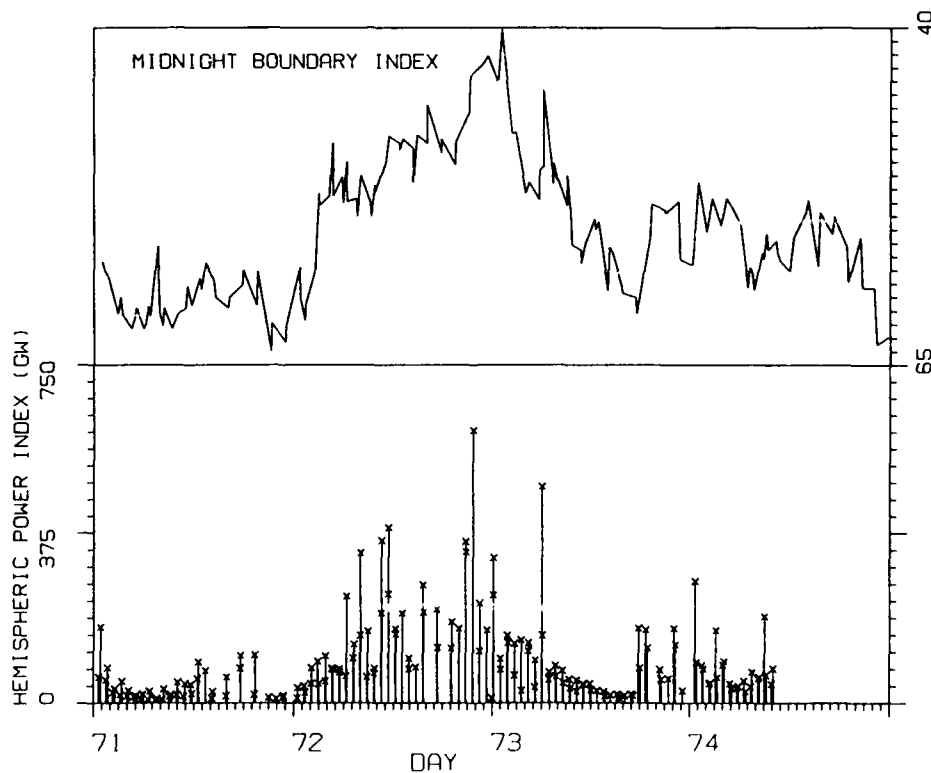


FIG. 2. Indices of geomagnetic activity for March 12-15 (Days 71-74) during the great storm derived from DMSP F8 and F9 precipitating-electron data. The Midnight Boundary Index is the location (degrees latitude) of the equatorward edge of the auroral electrons along the midnight meridian. The Hemispheric Power Index (gigawatts) is the total energy flux of energetic electrons flowing into one hemisphere.

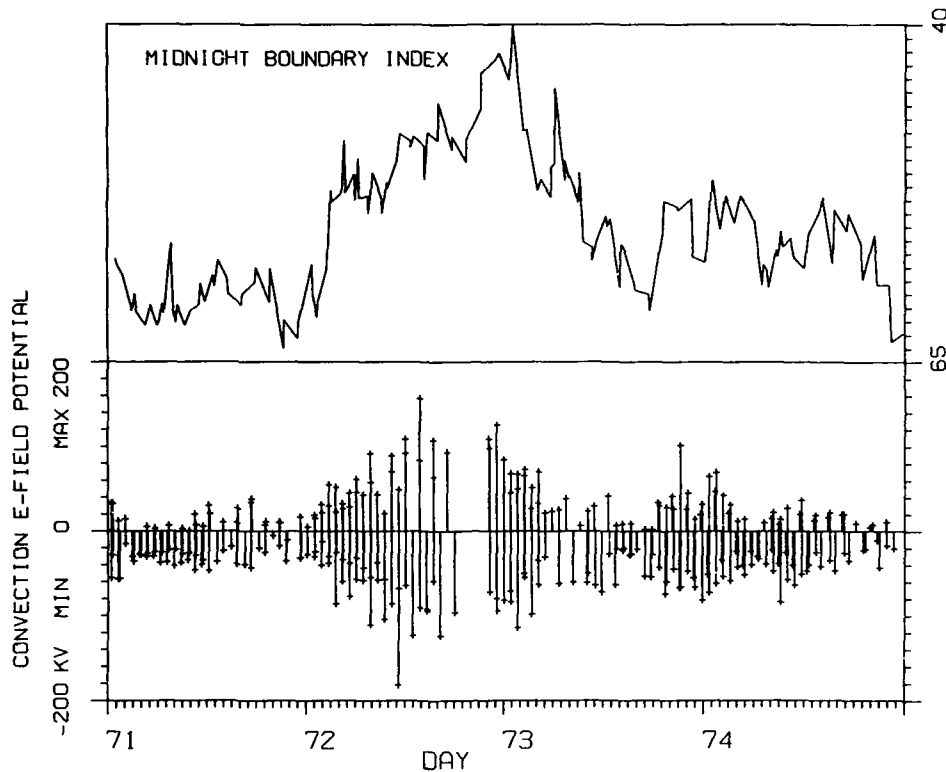


FIG. 3. The DMSP Midnight Boundary Index and the simultaneously observed maxima and minima in the convection electric-field potential (kilovolts) along the satellite track during the great storm. The maxima and minima potentials of the magnetospherically imposed electric field are slightly larger than the values observed along the satellite tracks. There was a gap in thermal-ion-drift data between 1700 and 2100 UT on Day 72.

saturated by the effects of the storm. Some of the effects of this storm at low and mid latitudes are described in other papers (4–6).

### Observations

#### Overview

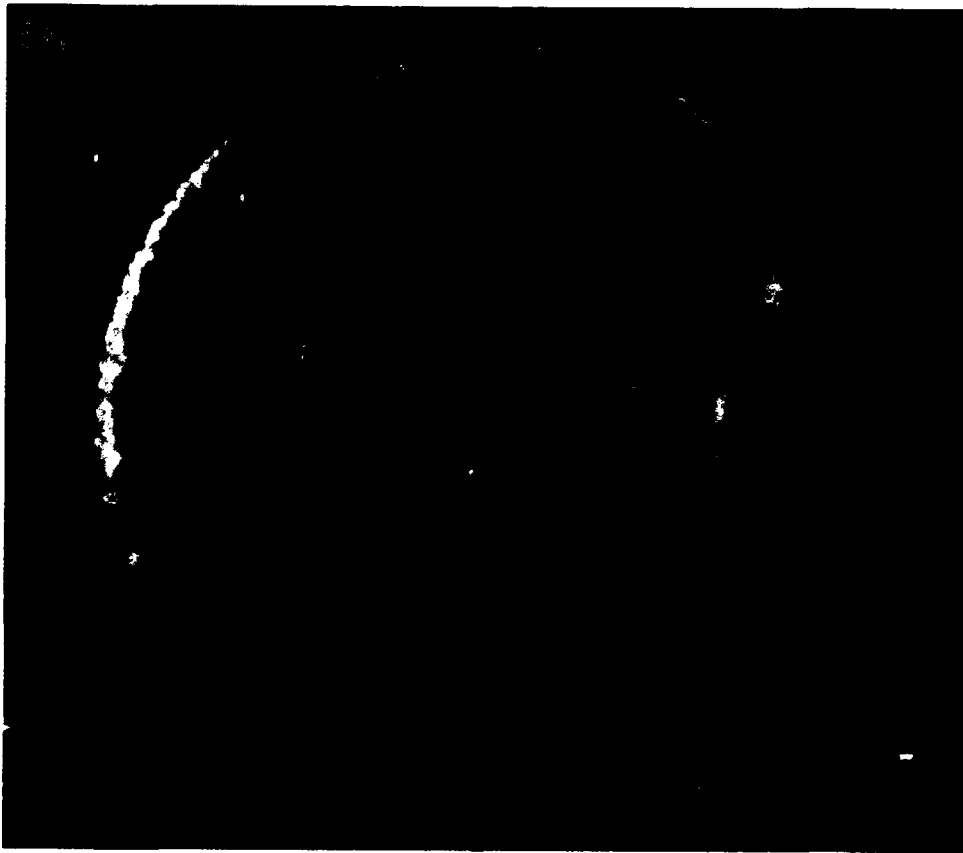
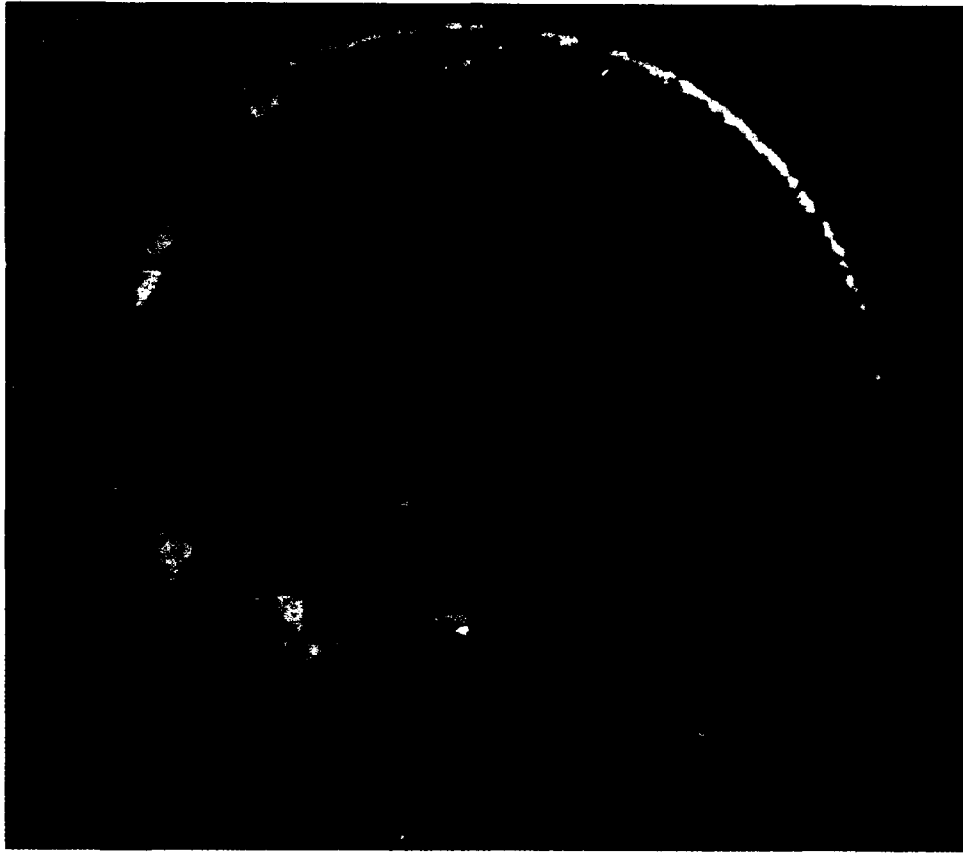
The storm began with a sudden storm commencement (SSC) event on March 13, 1989 (Julian Day 72) at 0128 UT. The standard indices of geomagnetic activity are shown in Fig. 1. The indices show that the magnetosphere was already in a disturbed condition due to energy input from a set of storms occurring a few days before the great storm. The auroral electrojet (AE) and  $K_p$  indices increased quickly to very high levels immediately following the SSC and maintained a roughly steady value for the next 30 h. The disturbance with storm time ( $D_{st}$ ) index steadily rose during Day 72 until it peaked 23 h after the SSC. Solar wind and IMF data from the IMP satellite were not available until midday of Day 73 when the IMF was strongly northward. This northward direction was probably responsible for the relative lull in the high- and mid-latitude activity. The  $K_p$  and AE indices rose again when the IMF turned southward sometime late on Day 73 indicating that more energy was again flowing into the outer magnetosphere. The  $D_{st}$  index rose only slightly when the IMF turned southward indicating that little of the second wave of energy into the outer magnetosphere penetrated into the inner magnetosphere.

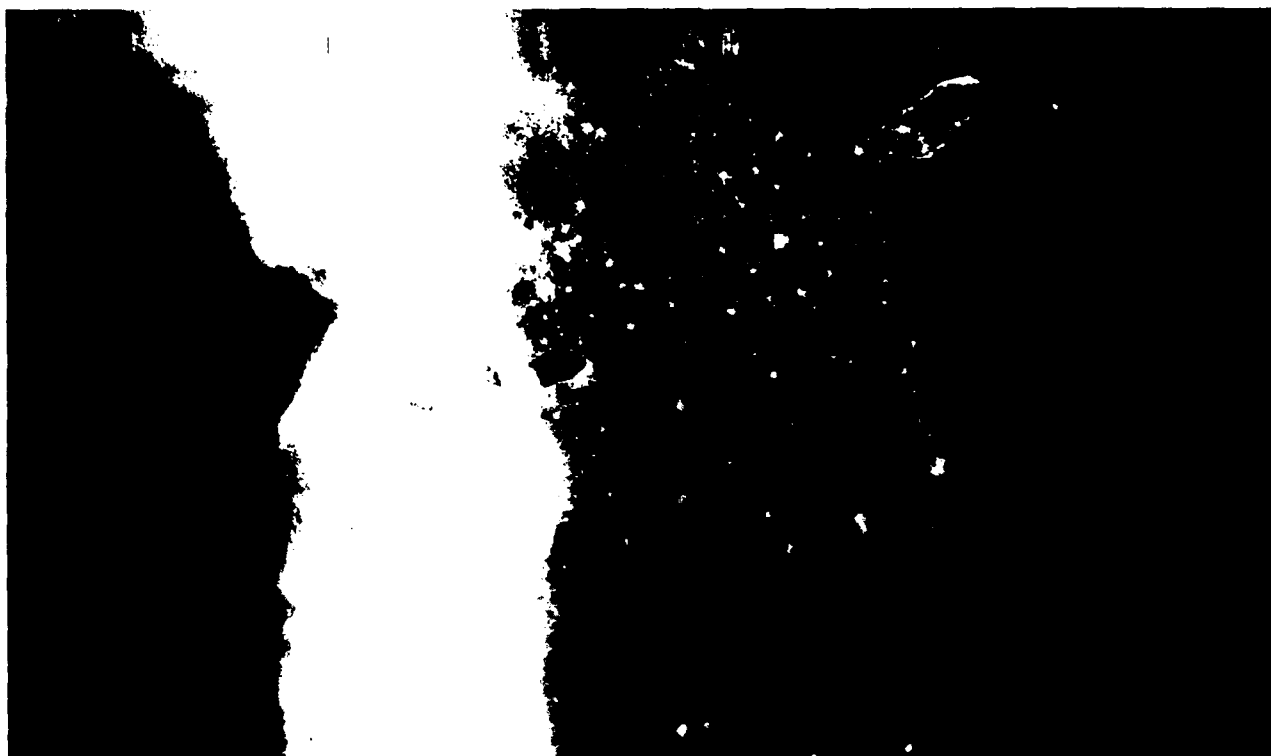
#### DMSP and DE data

The DMSP has provided a continuing series of U.S. Air Force satellites in low Earth orbit. While the primary mission is to observe the troposphere, the white-light imager is able to detect the aurora at night. The DMSP satellites also carry precipitating-particle spectrometers (7) and thermal plasma monitors (8) to observe the ionosphere–magnetosphere interaction. The particle spectrometer (acronym SSJ/4) detects precipitating ions and electrons with pitch angles near the local vertical direction within 20 logarithmically spaced energy channels from 30 eV to 30 keV. The thermal plasma monitor (acronym SSI/ES) measures the vertical and cross-track components of the ionospheric bulk flow and measures the total thermal-ion density at the satellite. At the time of the March 1989 storm, two DMSP satellites, (F8) and (F9) were operating. Both satellites were in a 840 km altitude circular, Sun-synchronous, polar orbits. The F8 and F9 satellites have ascending and descending nodes at local times of 0600–1800 and 1030–2230 h, respectively. Dynamics Explorer 1 is one of a pair of NASA scientific research satellites launched in 1981 that has an elliptical polar orbit of 23 000 by 700 km. At the time of the March 1989 storm, the UV imager (9) was one of a few instruments still operating and apogee for DE-1 was over the south pole.

The time history of the March 1989 storm can be followed by using indices built from the 30 eV–30 keV precipitating-electron data from the two DMSP satellites, Fig. 2. The mid-

FIG. 4. (a) Image of Earth obtained with DE UV imager at 0150 UT on March 14, 1989 at 82° S, 55° W, 20 000 km altitude showing the aurora over the southern hemisphere. The map of coastlines is superposed upon the image. (b) The image of the aurora over the northern hemisphere was made by mapping the observed pixels along the Magsat model geomagnetic field lines to points in the magnetically conjugate points in the northern hemisphere.





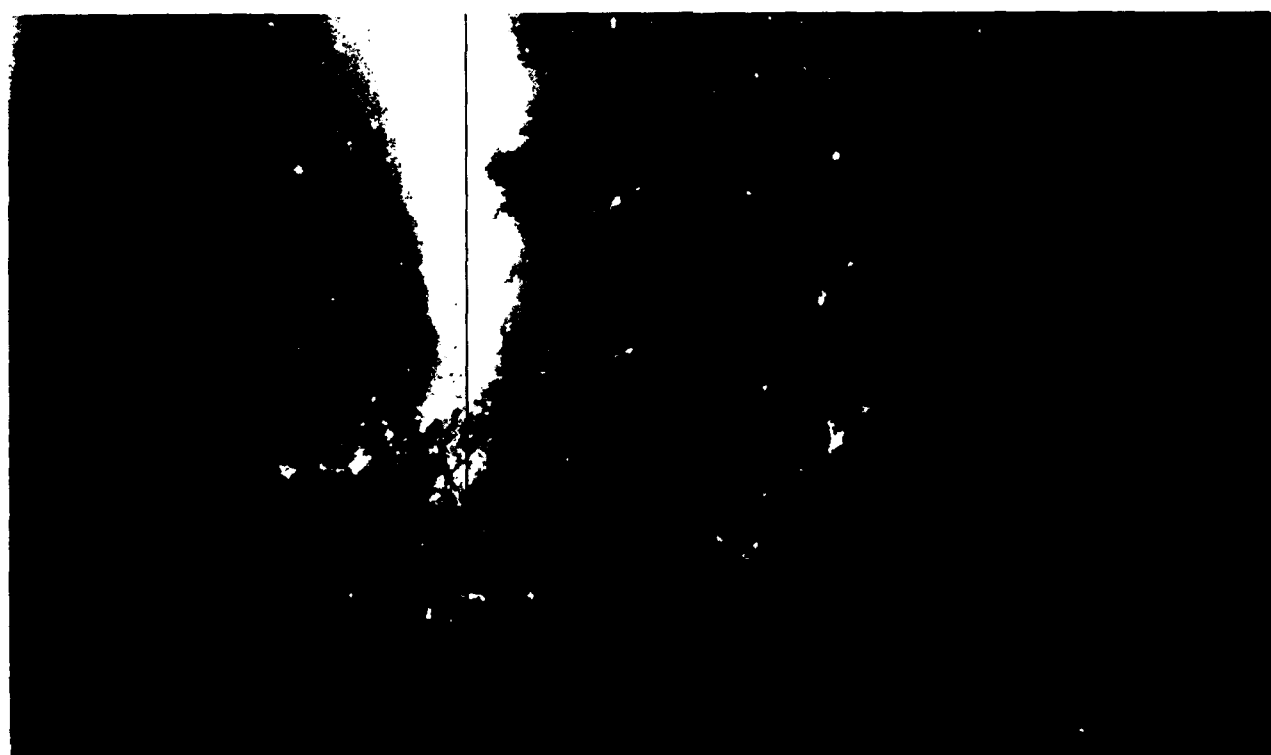
04:04:00Z  
 LAT 49.82N  
 LON 118.05W  
 W0549 R+07  
 PLS X11  
 MDR3 TC39

04:01:19Z  
 LAT 49.60N  
 LON 117.92W  
 W0549 R+07  
 PLS X11  
 MDR3 TC39

03:58:30Z  
 LAT 49.65N  
 LON 118.77W  
 W0549 R+07  
 PLS X11  
 MDR3 TC39

03:55:41Z  
 LAT 49.43N  
 LON 118.67W  
 W0549 R+07  
 PLS X11  
 MDR3 TC39

03:52:57Z  
 LAT 49.32N  
 LON 118.69W  
 W0549 R+07  
 PLS X11  
 MDR3 TC39



05:45:37Z  
 LAT 49.82N  
 LON 118.05W  
 W0549 R+08  
 PLS X11  
 MDR1 TC49

05:42:45Z  
 LAT 49.80N  
 LON 117.88W  
 W0549 R+08  
 PLS X11  
 MDR1 TC49

05:39:56Z  
 LAT 49.65N  
 LON 118.77W  
 W0549 R+08  
 PLS X11  
 MDR1 TC49

05:37:07Z  
 LAT 49.43N  
 LON 118.67W  
 W0549 R+08  
 PLS X11  
 MDR1 TC49

05:34:18Z  
 LAT 49.32N  
 LON 118.69W  
 W0549 R+08  
 PLS X11  
 MDR1 TC49

night auroral boundary index (MABI) (10–12) follows the equatorward edge of the precipitating electrons. This boundary is the ionospheric projection of the inner edge of the magnetospheric plasma sheet. Since the latitude of the auroral oval varies with the local time, the observed equatorward boundaries are normalized to the midnight meridian using an average shape for the auroral oval. The MABI can be used to follow geomagnetic activity during a storm (cf. ref. 13). For this storm, the MABI dropped sharply at the beginning of March 13, 1989 and continued to decline during the day. At 0103 UT on March 14, 1989, the MABI reached a minimum of  $40.1^\circ$  or  $L = 1.71$ . By comparison, during a "typical" storm, the lowest latitude at which precipitation is observed directly or indirectly is approximately  $L = 2.5 \pm 0.5$  (14) or magnetic latitude =  $50.7^\circ + 4^\circ - 5.7^\circ$ . After 0103 UT on March 14, 1989, the MABI recovered in a manner similar to the recovery of the  $D_{st}$  index.

Figure 2 also shows the hemispheric power index. This is an estimate of the total energy flux of precipitating electrons into one hemisphere based upon the observed energy flux of precipitating electrons. The algorithm for calculating the total energy flux is based on a set of NOAA-Tiros statistical maps of electron energy fluxes at auroral latitudes (15, 16). The DMSP particle data are normalized according to how the satellite trajectory crosses these statistical maps. The index is calculated twice per orbit under optimum conditions.

The DMSP thermal plasma monitor includes an ion driftmeter that measures the cross-track component of ionospheric plasma convection. Assuming the plasma is collisionless and thus "frozen" to the magnetic flux tubes, the relationship  $E = v \times B$  is used to determine the component of the convection electric-field parallel to the satellite track. By integrating this electric-field component, we calculate the distribution of the electrostatic potential across the high-latitude ionosphere (17) if there are no significant data gaps and if the satellite completely crosses the auroral zone. Figure 3 includes the minimum and maximum potentials measured at high latitudes by the F8 and F9 satellites during the March 1989 storm. These data have not been corrected for the satellite trajectory. The F8 orbit tracks are parallel to the dusk-dawn meridian. Since the maximum and minimum potential of the global convection electric field are near  $\sim 5$  and  $\sim 17$  h, the F8 measured minimum and maximum is usually close to the minimum and maximum in the global convection pattern. The F9 orbit tracks are parallel to the 1030–2230 h local time meridian. Since the zero-potential contour is roughly aligned with the noon-midnight meridian, the F9 orbit track is either to the dusk side or the dawn side of the zero-potential contour. Thus either the F9 measured minimum or a maximum potential is close to the minimum or maximum potential for the global pattern, and the other extrema is not meaningful. In general, the potentials plotted in Fig. 3 represent at least 75% of the maximum or minimum for the global pattern.

Approximately 1 h after the peak in the storm, the UV imager on the DE satellite obtained an image of the very bright and greatly extended aurora over the southern hemisphere (Fig. 4a). The UV emission between 1360 and 1650 Å ( $1 \text{ \AA} = 10^{-10} \text{ m}$ ) are due to nitrogen molecules near 200 km altitude excited by

energetic (1–10 keV) precipitating electrons. On the limb of the Earth, the imager detected emissions from the atmospheric molecules excited by sunlight. Because the aurora is a response to a magnetospheric source that sends approximately equal fluxes of particles into both hemispheres, it is reasonable to estimate what the aurora looked like over the northern hemisphere. Figure 4b was created by using the Magsat model geomagnetic field to project the observed UV luminosity onto the magnetically conjugate points. From this mapped image, it is easy to understand the sightings of the aurora at low-latitude locations such as Jacksonville, FL; Dallas, TX; and Phoenix, AZ. A significant feature of the aurora was that the aurora in the midnight sector seemed to be split into two bands; this will be discussed later in the paper. There were a few other DE images of the aurora during the storm but they are not presented in this report.

The DMSP white-light, line-scanning imager on F9 obtained images of the aurora across North America a few hours after the peak in geomagnetic activity and shortly after the DE image (Fig. 5). Owing to the low altitude of the DMSP satellites, each image shows only a portion of the aurora. Thus two consecutive orbit are required to show all of North America. None of the F8 images show the aurora because the image was saturated with sunlight during this season.

In Fig. 6, we show a map of the world overlaid with the DMSP orbits during the early hours of March 14, 1989. The portions of the orbits where the precipitating electron flux was sufficient to generate visible aurora have been colored yellow. By comparing the F8 and F9 passes near 0105 and 0218 UT with the DE image in Fig. 4 at 0151 UT, we see an excellent correlation between the two data sets. Thus we are confident that the two satellites were observing the same auroral structure and look into the DMSP data for the explanation of the dark region between the equatorward and poleward portions of the aurora as seen in the DE image. As an additional check, we use the precipitating-electron data and white-light image (Fig. 5) for the F9 pass near 0356 match.

The DMSP precipitating particle and thermal ion drift data are shown in more detail in Fig. 7 so that we can show the similarities and difference between observations during this great storm and observation that would be made during an ordinary storm (maximum  $K_p \sim 6$  or 7). By chance, during March 1989, the F8 and F9 spacecraft were crossing the same hemisphere at almost the same time. The data in Fig. 7a were obtained from a southern hemisphere pass approximately 1/2 h before the DE image and exactly at the peak of the storm according to the MABI. A quick glance at the precipitating particle data without looking at the latitudes on the scale does not show anything that could not be found in any period when the IMF  $B_z$  component is negative and a substorm is in progress. (Note that the low-latitude data, especially for F9 in Fig. 7a are slightly contaminated by radiation belt particles.) After consulting the latitude scales, one notes that the region of intense electron precipitation associated with the auroral zone is both broader and at lower latitudes than under more normal conditions. However the average energy and the energy flux ( $\text{ergs cm}^{-2}$ ) are about the same as seen during a strong substorm embedded in an average geomagnetic storm. In the ion-drift

FIG. 5. Images of Earth obtained with DMSP F9 white-light imaging linescanner over North America near 0356 and 0537 UT on 14 March 89. The track of the satellite from north to south is the center of each image from top to bottom. City lights and geographic features in North America can be seen.

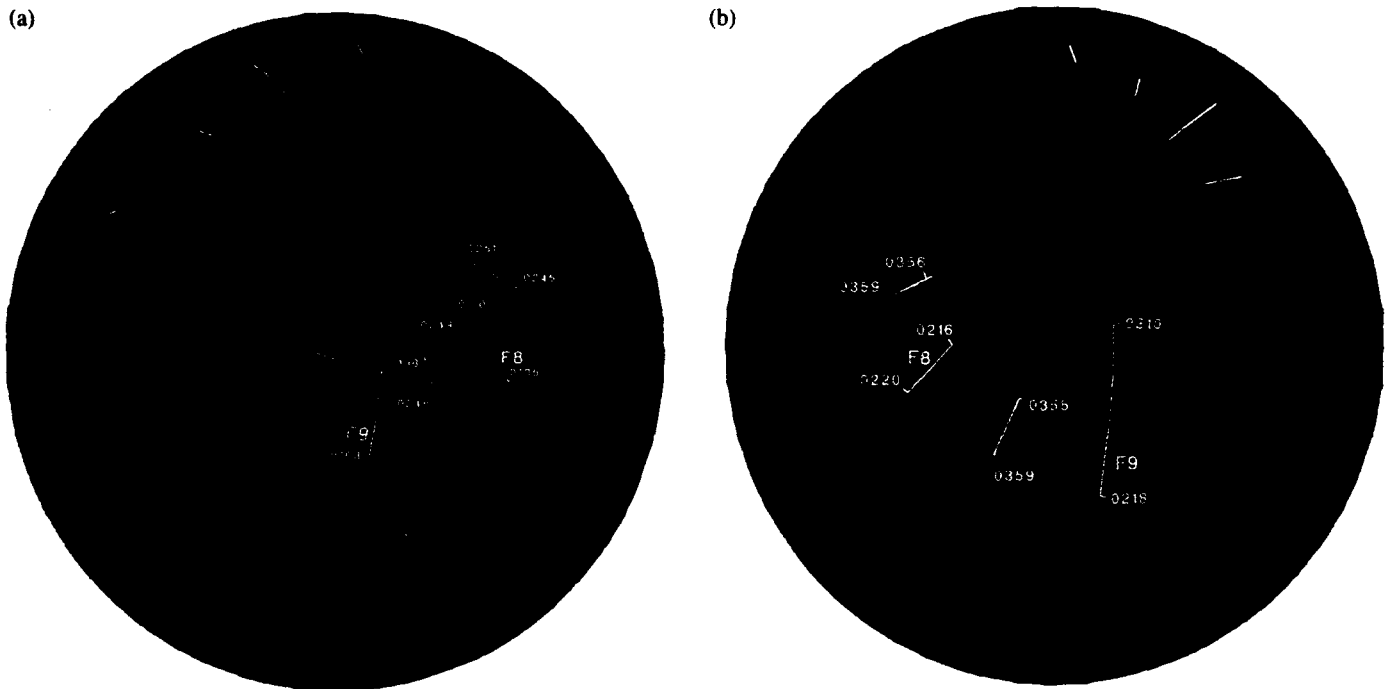


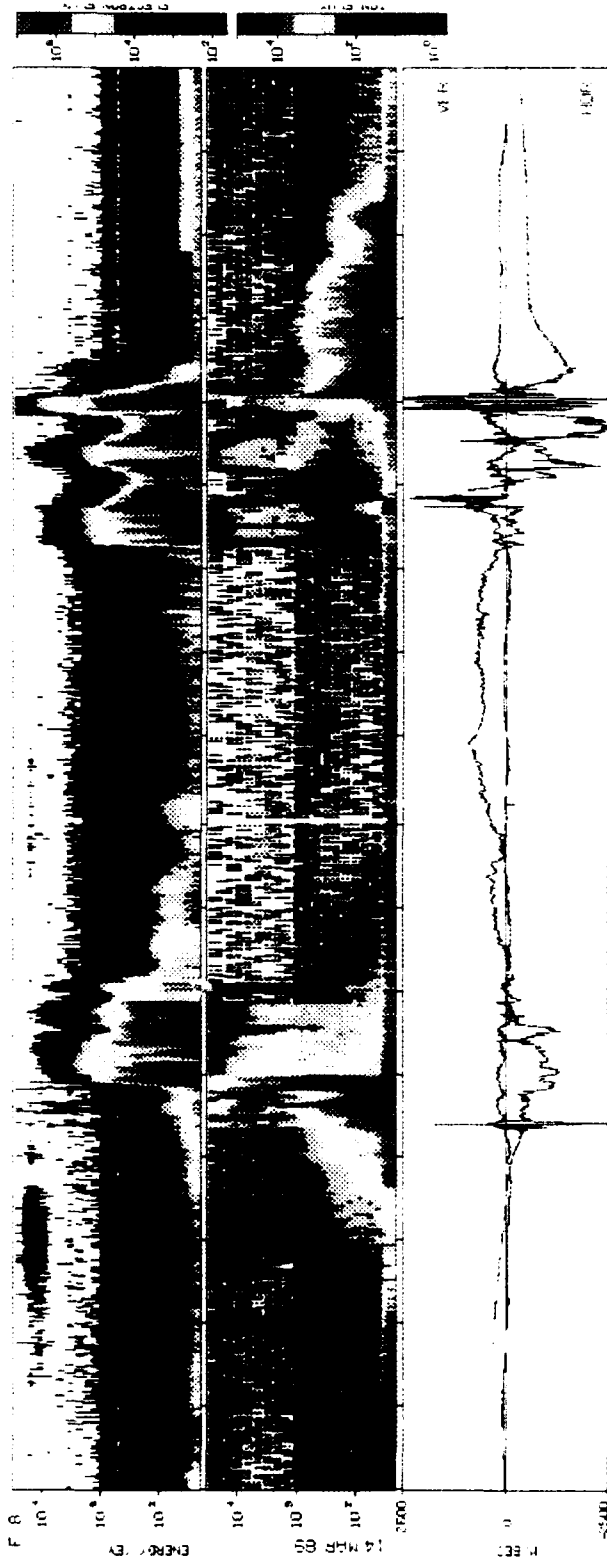
FIG. 6. Map of (a) the Southern Hemisphere and (b) the Northern Hemisphere with the DMSP F8 and F9 ground tracks shown for early on 14 March 89. The projections shown were chosen to approximate the DE images shown in Fig. 4. The portion of the DMSP tracks where precipitating electrons energetic enough to create visible aurora are shown as yellow lines; regions with soft or no electron precipitation are shown as black lines.

data, the sunward flows (negative values for the red line) in the aurora zones are large but the flow is not any faster than would be observed during a small or moderate storm. Since the ion drift is directly related to the convection electric field and the auroral electron-energy flux is closely related to the ionospheric conductivity, we estimate that the height-integrated auroral current density (amp per metre) was approximately the same during this storm as it would be during a minor storm. This estimate is supported by the fact that the AE index was not higher during this storm than it would be during a minor storm. The latitude and the latitudinal width of the flows are extraordinarily low and wide, respectively. Because of the latitude change, the auroral displays and other "high" latitude effects of this storm were closer to population centers, especially in the northern hemisphere. Owing to the increased width of the auroral zone, the total energy deposited and the total auroral current were much larger than observed in a minor storm.

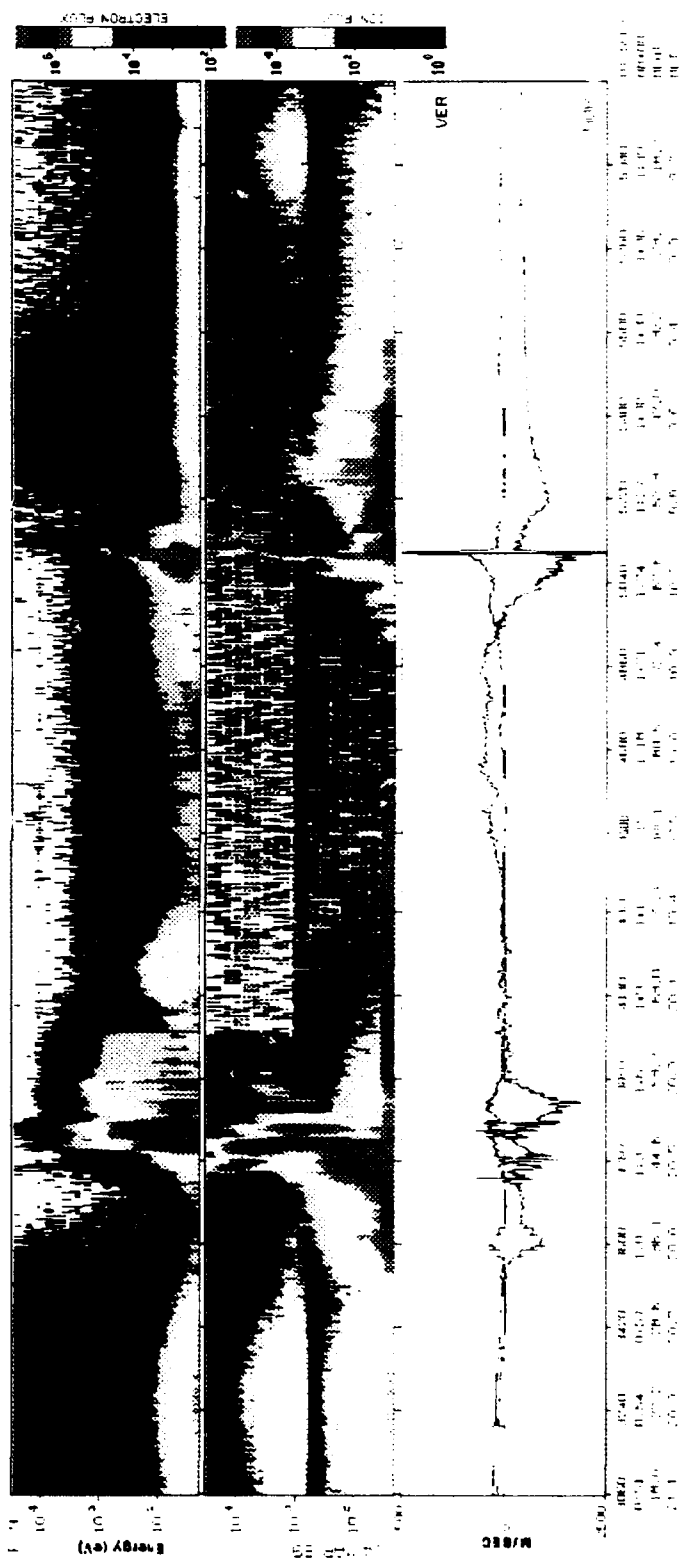
There are several features in the data that are different from the features observed during a minor storm or a period of strong substorms. There was a series of large-amplitude, small-scale disturbances in the east-west thermal ion drift, which were

related to the north-south component of the electric field. Although disturbances like these can be found in the data during moderate activity, they are rare events except near the dayside cusp. We will identify these disturbances as regions of very strong ultra low frequency (ULF) wave activity, but due to the quick passage of the spacecraft through the regions, we cannot clearly identify the spectrum of the waves. An unusual feature of the ion-drift data is the occurrence of upward (positive values for the blue line) flows greater than  $1000 \text{ m s}^{-1}$ . Typically the upward-flow speed over the aurora zones is  $100\text{--}400 \text{ m s}^{-1}$  owing to the heating of the thermal ions by the precipitating particles (especially electrons with energies between 100 eV and 1 keV), field-aligned currents, and wave-particle interactions. The presence of faster than normal upward ion flows indicates stronger than normal heating of the topside ionosphere. Since the fastest flows of thermal ions were often seen near regions of wave activity, as indicated by the east-west drift data, we conclude that the wave activity and the upward flow are part of a single physical mechanism. There are insufficient data from these observations alone to determine that the link is the waves heating the topside ionosphere, or intense

FIG. 7. (a) Precipitating-electron and ion data and thermal-ion drift data from nearly simultaneous southern hemisphere high-latitude passes of the DMSP F8 (top three panels) and F9 (bottom three panels) spacecraft starting at 0051 UT on March 14, 1989. The precipitating-electron (top panel and fourth panels) data and the precipitating-ion data (second and fifth panels) are shown as a color spectrogram of number flux (particles  $\text{cm}^{-2} \text{ s}^{-1} \text{ keV}^{-1}$ ) vs. energy and time. The ion-drift (third and sixth panels) data are line plots with the red line indicating the cross-track (approx. east-west) ion drift ( $\text{m s}^{-1}$ ) and the blue line indicating the vertical ion drift. Corotation has not been subtracted from the measured cross-track ion drift. (b) Same as (a) except for nearly simultaneous F8 and F9 northern hemisphere passes beginning at 0142 UT March 14, 1989. (c) Same as (a) except for nearly simultaneous F8 and F9 southern Hemisphere passes beginning at 0236 UT March 14, 1989. (d) Same as (a) except for nearly simultaneous F8 and F9 northern hemisphere passes beginning at 0327 UT March 14, 1989.



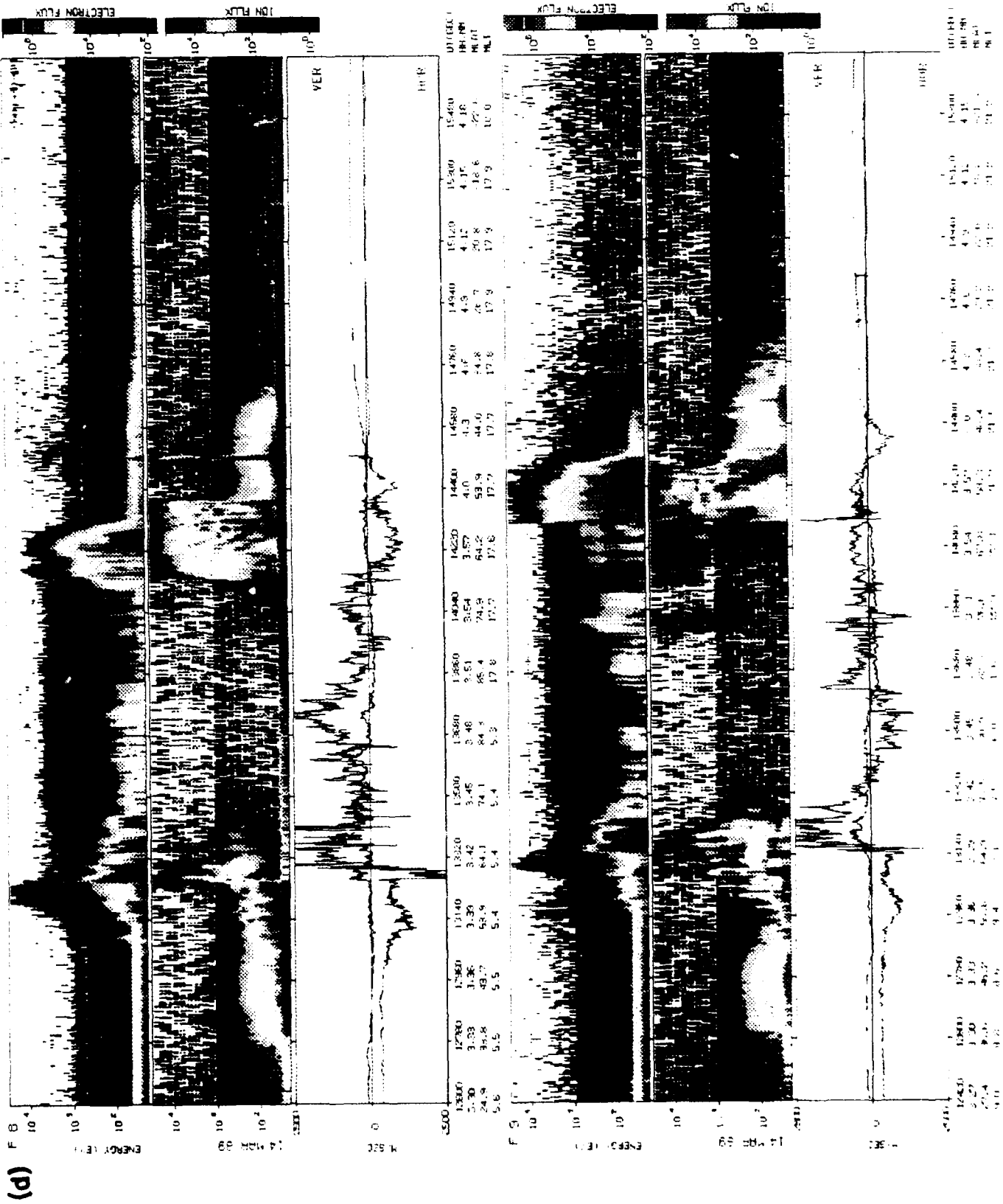
(a)



(b)



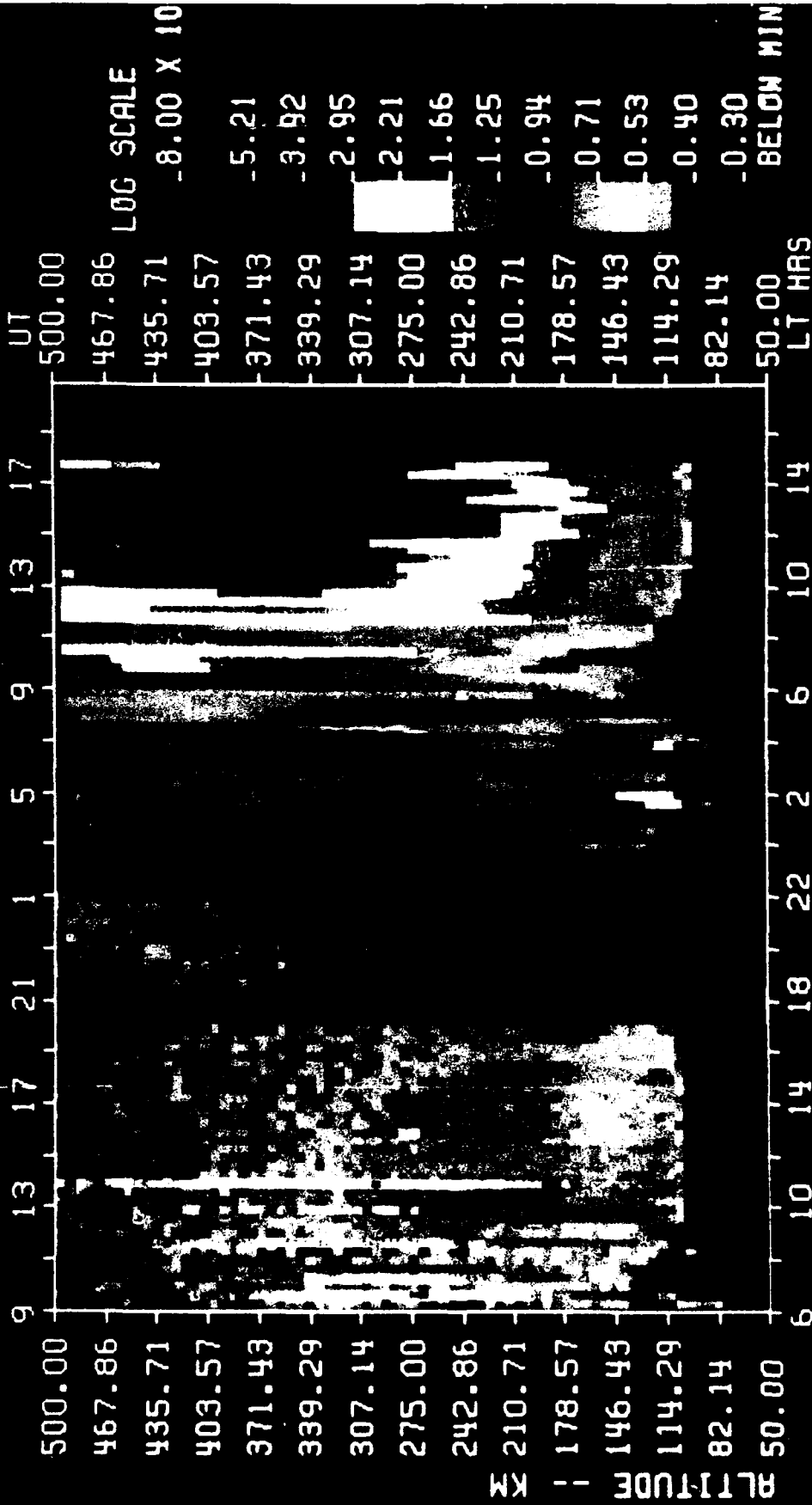






890313 T0 890314 SONDRESTRØM

091015 175235 UT



PHYNAL NE EL/CM\*\*3 UP B

SRI90AE66

if the soft ions have been injected from the soft-ion population in the central plasma sheet or if they are plasmaspheric ions that have been energized. It has been observed that 10–50 keV  $O^+$  ions from the ring current precipitate into the mid-latitude ionosphere for several days after a storm (25) and disturb the mid-latitude ionosphere (21). Thus it is possible that these soft ions were heated by interaction of the thermal plasmasphere ion with the ring current.

The data shown in Fig. 7c and 7d indicate a continuation of the shrinkage of the auroral oval's diameter and of the width of the auroral oval, although the auroral boundary was still well equatorward and wider than normal. The data on the right side of Fig. 7d were obtained simultaneous with the white light image shown in Fig. 5.

#### Sondre Stromfjord ICS radar data

The incoherent radar station at Sondre Stromfjord was operated on 0903 UT on March 13 to 1803 UT on March 14 and from 2329 UT on March 15 to 0509 UT on March 16. In Fig. 9, the observed electron-density profiles for the central portion of the storm are presented. The most remarkable feature of the density profiles is that the density was a bit lower than normal on March 13 during the maximum of the storm and was enhanced on March 14 after the indices had begun to decline from their maximum levels. In addition, the radar was able to measure the local ion-drift velocities (not shown). The most notable feature of the ion-drift data is that the drifts in the local noon sector (1500 UT) were predominately eastward on March 13 and were predominately westward on March 14. This indicates a change in the sign of the IMF- $B_y$  component between the two times.

#### Other data

Figure 10 shows a sampling of  $f_0F_2$  data from just before the storm to near the end of the storm. The electron density at the altitude of maximum density ( $F_2$ ) at the middle latitude and low latitude was decreased during the storm. Since the ion density at the DMSP altitude (840 km) was increased at the same time, we conclude that the altitude of the  $F_2$  peak increased substantially on a global basis. The magnetosphere electric field can accomplish this by penetrating the usual shielding (Alfvén) layer. In addition, gravity waves launched from the auroral zone modify the low- and middle-latitude ionosphere in a complex manner.

There are many other data sets that we intended to present in this review of ionospheric data but we are not able to present them. For example, limited data from the HILAT satellite exist, but do not add significantly to the information available from DMSP. Some data from the EXOS-D satellite were recorded, but the data had not been processed at the time of submission to the journal. The particle spectrometers on the NOAA/Tiros were not operating in a mode that allowed useful data to be collected. The Goose Bay ionosonde was so overwhelmed with E-region echoes that the F-region could not be characterized. There were other data sources but they were not readily available. Even if we had obtained all possible data, we would be working with a sparse data set. Most of the processes in the geospace environment occur on smaller time and spatial scales than the existing observing stations and satellites.

## Discussion

The UV image obtained with the DE-1 satellite shown in Fig. 4 has been very widely disseminated, including the front cover of the *EOS* issue containing Allen's article (1). The dark band between the two bright bands of auroral luminosity near midnight has appeared to some casual observers as an abnormal configuration of the auroral zone. However, such observations miss two important points. The structure in Fig. 4 was a snapshot of a dynamic event and the dark band was not really dark, but was darker (at least in the UV spectrum) than adjoining parts of the auroral zone. The bright band on the poleward side of the auroral zone had the typical shape for the poleward surge in the midnight sector during the breakup stage of a substorm. The bright bands result from accelerated electrons associated with upward field-aligned currents while the darker band was dimly illuminated by unaccelerated electrons associated with downward field-aligned currents. Although the F9 satellite was slightly to the west of the midnight sector and passed through the auroral zone 20 min later, the DMSP data support this concept. The energy flux of precipitating electrons at 0211–0217 UT in the 1–10 eV range was roughly uniform, but the energy flux of the 100 eV–1 keV electrons dropped by a factor of 3 between 0212 and 0213 UT. While the soft electrons did not cause the UV emission observed by the DE-1 instrument, they could be a fossil of a similar fluctuation in the energy flux of the 1–10 keV electrons at the time of the DE-1 image. There could be another explanation of the dark band between the two bright bands of the DE-1 image, but nothing in the DMSP data supports a bifurcation of the auroral zone.

The AE index is often considered as the best indicator of high-latitude activity. At low to moderate levels of activity it has been found that the AE index scales approximately linearly with the energy input from the solar wind. At high levels of energy flow from the solar wind, Weimer *et al.* (26) found that the  $\partial(AE)/\partial(IMF B_y)$  decreased and that there was an indication that the magnitude of AE, and in turn the strength of the auroral electrojet, could not exceed some maximum level. In other words, the current density of the auroral electrojet has a saturation level. Since it had been found that there was a linear relationship between the AE index and the cross polar-cap potential obtained from ground-based data (27) and satellite-based data (28), Weimer *et al.* postulated that the cross polar-cap potential also saturates. If this were the case, then the observed potential during this storm should have been in the range of 120–160 kV. However, from Fig. 3 we estimate that the cross cap potential had a value of 200 kV or more from approximately 0700 UT on March 13 until 0400 UT on March 14, and it exceeded 300 kV near 1300 UT on March 13. Thus data from this storm indicate that the cross polar-cap potential either does not saturate or it would saturate at a much higher level of energy input from the solar wind than did the auroral electrojet current.

## Conclusions

(i) The major features of the great storm of March 1989 were the same as one would observe during a minor storm. The difference is that the magnitude of many but not all the features were increased from normal storm values. The split in the UV luminosity was probably due to a normal variation in the aver-

FIG. 9 (Opposite). Observations of electron density as a function of time and altitude along the magnetic field line over Sondre Stromfjord. These data were obtained with the incoherent scatter radar from 0190 UT on March 13, 1989 to 1752 UT on March 14, 1989. The densities are color coded from  $0.3 \times 10^5$  to  $8.0 \times 10^5$  electrons  $cm^{-3}$ .

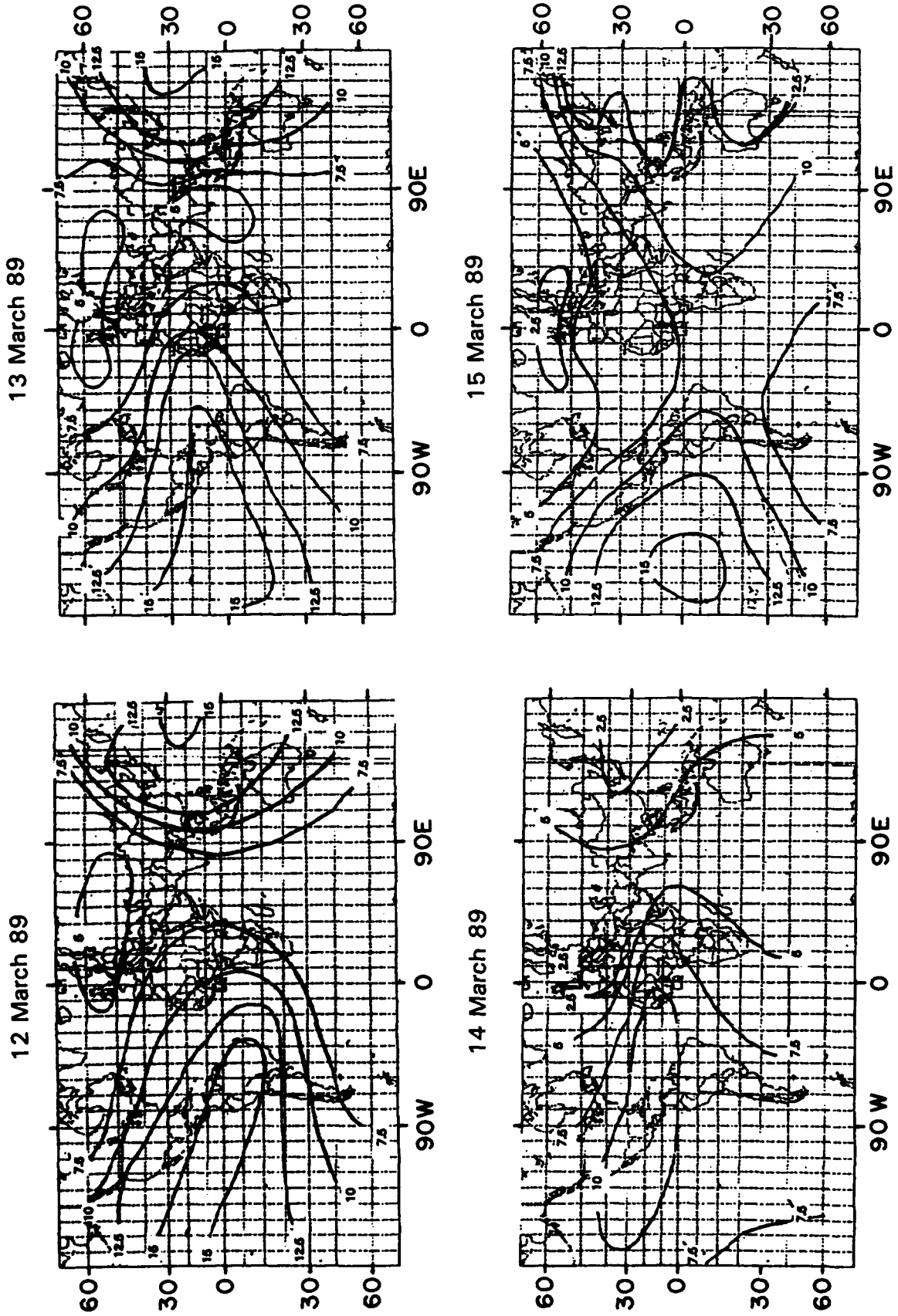


FIG. 10. Contours of  $f_oF_2$  (MHz) at 0000 UT for each day of March 12-15 1989 determined from ionosonde stations at low- and mid-latitudes.

age energy of precipitating particles, and not to an unusual splitting of the auroral zone.

(ii) The magnitudes of various features of the storm did not all increase in the same ratio. The energy flux ( $\text{ergs cm}^{-2}$ ) of particles, the local auroral electric fields ( $\text{mV m}^{-1}$ ) and the auroral electrojet during the great storm were very similar to small storms. This is in agreement with previous reports of the saturation of the AE index. On the other hand, the total energy flux and the cross polar-cap potential increased as the width and breadth the auroral zone increased. There was no evidence that these latter two parameters saturated.

(iii) While only high-latitude regions (including latitudes that are normally considered as part of the mid-latitude region) were directly affected by the input of energy from the magnetosphere, the ionosphere at all latitudes was affected by the storm.

#### Acknowledgements

The Dynamics Explorer UV image of the aurora was provided by Professor Louis Frank of University of Iowa. The  $f_0 F_2$  data were provided by Professor K. C. Yeh of the University of Illinois at Urbana-Champaign. The  $D_{st}$  data were provided by World Data Center - C. This work was supported by the Air Force Office of Scientific Research Task 2311G5. We thank Dr. M. S. Gussenhoven and Mr. D. Madden for assistance with the DMSP particle data and Mrs. J. James for assistance with the DMSP thermal plasma data.

1. J. Allen, H. Sauer, L. Frank, and P. Reiff. *EOS Trans. Am. Geophys. U.* **65**, 1479 (1989).
2. D. H. Boteler. *EOS Trans. Am. Geophys. U.* **72**, 159 (1991).
3. S. Musman. *Proc. ION-89*, Inst. Navigation, Washington, D.C., 421, 1989.
4. M. E. Greenspan, C. E. Rasmussen, W. J. Burke, and M. A. Abdu. *J. Geophys. Res.* **96**, 13 931 (1991).
5. I. S. Batista, E. R. de Paula, M. A. Abdu, N. B. Trivedi, and M. E. Greenspan. *J. Geophys. Res.* **96**, 13 943 (1991).
6. Y.-N. Huang and K. Cheng. *J. Geophys. Res.* **96**, 13 953 (1991).
7. F. J. Rich, D. A. Hardy, and M. S. Gussenhoven. *EOS Trans. Am. Geophys. U.* **66**, 513 (1985).
8. M. E. Greenspan, P. B. Anderson, and J. M. Pelagatti. *Tech. Rep. AFGL-TR-86-0227*, Hanscom AFB, Bedford, MA, 1986.
9. L. A. Frank, J. D. Craven, K. L. Ackerson, M. R. English, R. H. Eather, and R. L. Carovillano. *Space Sci. Instrum.* **5**, 369 (1981).
10. M. S. Gussenhoven, D. A. Hardy, and N. Heinemann. *J. Geophys. Res.* **88**, 5692 (1983).
11. D. A. Hardy, M. S. Gussenhoven, and E. Holeman. *J. Geophys. Res.* **90**, 4229 (1985).
12. D. Madden, and M. S. Gussenhoven. *Tech. Rep. GL-TR-90-0358*, Hanscom AFB, Bedford, MA, 1990.
13. F. J. Rich, D. A. Hardy, R. H. Redus, and M. S. Gussenhoven. *J. Geophys. Res.* **95**, 7893 (1990).
14. A. S. Rodgers, G. L. Wrenn, and H. Rishbeth. *J. Atmos. Terres. Phys.* **51**, 851 (1989).
15. J. C. Foster, J. M. Holt, R. G. Musgrove, and D. S. Evans. *Geophys. Res. Lett.* **13**, 656 (1986).
16. T. J. Fuller-Rowell and D. S. Evans. *J. Geophys. Res.* **92**, 7606 (1987).
17. R. A. Heelis and M. R. Hairston. *Tech. Rep. GL-TR-90-0047*, Hanscom AFB, Bedford, MA, 1990.
18. M. E. Greenspan, C.-I. Meng, and D. H. Fairfield. *J. Geophys. Res.* **91**, 11 123 (1986).
19. P. T. Newell, and C.-I. Meng. *J. Geophys. Res.* **95**, 7869 (1990).
20. J. T. Gosling, D. N. Baker, S. J. Bame, and R. D. Zwickl. *J. Geophys. Res.* **91**, 11 352 (1986).
21. K. Makita and C.-I. Meng. *J. Geophys. Res.* **92**, 7381 (1987).
22. J. T. Gosling, S. J. Bame, D. J. McComas, and J. L. Phillips. *Geophys. Res. Lett.* **17**, 901 (1990).
23. P. T. Newell and C.-I. Meng. *J. Geophys. Res.* **91**, 11 133 (1986).
24. W. Swider. *J. Geophys. Res.* **95**, 10 417 (1990).
25. P. H. Smith, N. K. Bewtr, and R. A. Hoffman. *J. Geophys. Res.* **86**, 3470 (1981).
26. D. R. Weimer, L. A. Reinleitner, J. R. Kan, L. Zhu, and S.-I. Akasofu. *J. Geophys. Res.* **95**, 18 981 (1990).
27. B.-H. Ahn, S.-I. Akasofu, Y. Kamide, and J. H. King. *J. Geophys. Res.* **89**, 11 028 (1984).
28. D. R. Weimer, N. C. Maynard, W. J. Burke, and C. Liebrechi. *Planet. Space Sci.* **38**, 1207 (1990).